Polarized photon scattering off ^{52}Cr: Determining the parity of $J = 1$ states

Krishichayan,* Megha Bhike, and W. Tornow
Department of Physics, Duke University, Durham, North Carolina 27708, USA
and Triangle Universities Nuclear Laboratory, Durham, North Carolina 27708, USA

G. Rusev
Chemistry Division, Los Alamos National Laboratory, Los Alamos, New Mexico 87545, USA

A. P. Tonchev
Physics Division, Lawrence Livermore National Laboratory, Livermore, California 94550, USA

N. Tsoneva
Institut für Theoretische Physik, Universität Gießen, Heinrich-Buff-Ring 16, D-35392 Gießen, Germany
and Institute for Nuclear Research and Nuclear Energy, 1784 Sofia, Bulgaria

H. Lenske
Institut für Theoretische Physik, Universität Gießen, Heinrich-Buff-Ring 16, D-35392 Gießen, Germany
(Received 21 January 2015; revised manuscript received 19 March 2015; published 30 April 2015)

The photoresponse of ^{52}Cr has been investigated in the energy range of 5.0–9.5 MeV using the photon scattering technique at the HIγS facility of TUNL to complement previous work with unpolarized bremsstrahlung photon beams at the Darmstadt linear electron accelerator. The unambiguous parity determinations of the observed $J = 1$ states provides the basis needed to better understand the structure of $E1$ and $M1$ excitations. Theoretical calculations using the quasiparticle phonon model incorporating self-consistent energy-density functional theory were performed to investigate the fragmentation pattern of the dipole strength below and around the neutron-emission threshold. These results compare very well with the experimental values.

DOI: 10.1103/PhysRevC.91.044328 PACS number(s): 21.10.Re, 21.60.Jz, 23.20.Lv, 25.20.Dc

I. INTRODUCTION

Much experimental effort has been focused on measuring the low-lying magnetic ($M1$) and electric ($E1$) dipole strengths in nuclei across the nuclear landscape [1,2]. The observation of dipole states provides rich information on the various collective and single-particle nuclear excitation modes, in particular, pygmy dipole resonance (PDR) and spin-flip $M1$ resonance.

The concentration of $E1$ strength below or in the vicinity of the particle separation energy is commonly known as PDR, because of its weak strength in comparison with giant dipole resonance (GDR), which dominates the $E1$ strength in nuclei [3,4]. The origin of the PDR excitation is interpreted as the vibration of the neutron skin against the inert core of the nucleus and has been observed experimentally in deformed as well as spherical nuclei in medium- and high-mass regions [2]. However, not much detailed information on this low-energy $E1$ excitation is available in the mass $\sim$50 region. From an analysis of transition densities, the unique behavior of the PDR mode is revealed, making it distinct from the well-known GDR. The existence of the PDR mode near the neutron threshold also has important astrophysical implications. For example, reaction rates of (γ,n) and (n,γ) reactions in explosive nucleosynthesis of certain neutron-deficient heavy nuclei may be significantly enhanced by PDR [5]. Furthermore, for very neutron-rich exotic nuclei, PDR is an important topic of study at the new generation of radioactive ion-beam facilities.

$M1$ spin-flip resonance is another mode of dipole excitations involving nucleons that undergo a spin change and others that do not change their spin. This resonance is expected to appear typically around 8 MeV [1,6]. This mode is considered to split into two parts, an isoscalar and an isovector, respectively, on the lower and higher sides of the excitation energy. One famous example of such a resonance is the observation of $M1$ spin-flip excitation in ^{48}Ca ($N = 28$), where the $M1$ strength is essentially concentrated in a single strong transition [7,8]. The observation of the $M1$ mode of dipole excitation at the $N = 28$ shell gap provides a particularly intriguing example where the interplay of proton and neutron degrees of freedom can be explored in great detail [9,10]. When moving from the doubly-closed-shell ^{48}Ca nucleus ($Z = 20$, $N = 28$), the open proton $1f_{7/2}$ shell makes the $M1$ strength more complex and fragmentation emerges. Nuclei in the vicinity of the closed $N = Z = 28$ shell are another favorable region for observing a spin-flip $M1$ resonance, and according to the independent-particle model [11], a strong spin-flip $M1$ transition in these nuclei can be interpreted in terms of both proton and neutron $1f_{7/2}1f_{5/2}$ particle-hole excitations. The present nucleus ^{52}Cr lies in this region and differs from the doubly magic nucleus ^{56}Ni by four nucleons, having four fewer protons, i.e., $\pi 1f_{7/2}^{-4} \otimes \nu 1f_{7/2}$.

*krishi@tunl.duke.edu; krishichayan@gmail.com

A recent investigation [12] of the low-lying dipole structure in ^{52}Cr yielded information on several dipole excitations in this fp-shell nucleus using unpolarized bremsstrahlung and the nuclear resonance fluorescence (NRF) technique. However, because it is very difficult to obtain parity information with unpolarized bremsstrahlung beams, the lack of parity assignments hampers reliable interpretation of the observed $J = 1$ states in ^{52}Cr. In order to quantify the occurrence of electric ($E1$) and magnetic ($M1$) dipole excitations in ^{52}Cr, unambiguous parity determination is very crucial and, indeed, much needed.

The aim of the present work is to perform unambiguous parity assignments of the dipole excitations in ^{52}Cr, which is achieved in measurements of azimuthal asymmetries of nuclear resonance fluorescence γ rays using a 100% linearly polarized and quasimonochromatic photon beam. The experimental data are explained in detail using a microscopic theoretical approach based on energy density-functional (EDF) theory and the quasiparticle-phonon model (QPM) [13,14].

II. EXPERIMENTS

The current measurements were performed at the High Intensity γ-Ray Source (HIγS) facility of the Triangle Universities Nuclear Laboratory (TUNL) [15]. The HIγS facility produces a nearly monoenergetic, 100% linearly polarized (in the horizontal plane) photon beam through Compton backscattering of free-electron-laser photons with relativistic electrons stored in a storage ring. The photon beam was collimated by a lead collimator of length 30.5 cm with a cylindrical hole of 1.27-cm diameter before passing through the target. This collimation results in an energy spread of the photon beam of 3% (FWHM). The scattered γ rays from the natural Cr target of mass 6.48 g (the natural abundance of ^{52}Cr is 83.789%) were measured with an array of four HPGe detectors, each of 60% relative efficiency, positioned around the Cr target at $(\theta,\phi) = (90^\circ,0^\circ)$, $(90^\circ,90^\circ)$, $(135^\circ,45^\circ)$, and $(135^\circ,135^\circ)$, where θ is the polar scattering angle and ϕ is the azimuthal angle between the polarization plane of the beam and the direction of the scattered γ ray. The detectors were located 10 cm from the center of the target. A 123% efficient (relative to a standard $3'' \times 3''$ NaI detector) coaxial HPGe detector was placed downstream of the target position in order to measure the beam-energy distribution. During beam profile measurements, the beam was attenuated by a series of copper absorbers mounted upstream. An overview of the typical detector setup for parity measurements can be found in Ref. [16].

In its most general form [17,18], the measured azimuthal asymmetry of the scattered photons is given by

$$\epsilon = \frac{A_h - A_v}{A_h + A_v} = P_\gamma \Sigma, \tag{1}$$

where A_h and A_v are the corresponding efficiency-corrected count rates observed for the γ rays by detectors positioned horizontally and vertically to the scattering plane. P_γ is the polarization of the photon beam, which is assumed to be 1 for all energies at the HIγS facility. Therefore, the count-rate asymmetry ϵ will be equal to $+1$ for a $J_1^\pi = 1^+$ state decaying by an $M1$ emission to the ground state and -1 for a $J_1^\pi = 1^-$ state decaying by an $E1$ emission to the ground state. Experimental observations will deviate slightly from this, as the expressions given for ϵ do not account for the finite solid angles of the detectors and statistical uncertainties in the data.

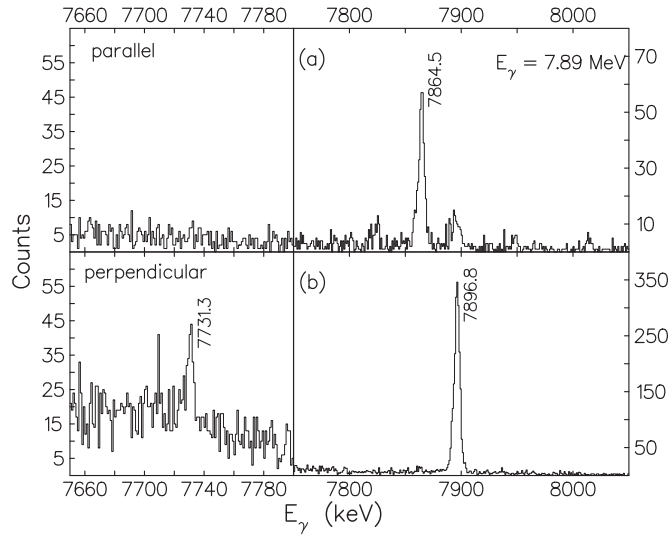

FIG. 1. Nuclear resonance fluorescence (γ,γ') spectra from ^{52}Cr recorded in the (a) parallel and (b) perpendicular detector using a polarized photon beam of energy 7.89 MeV. Transitions in the parallel (perpendicular) detector are of an $M1$ ($E1$) character.

III. DATA ANALYSIS AND RESULTS

The dipole excitation strength distribution in ^{52}Cr has recently been measured with unpolarized bremsstrahlung up to $\sim$10 MeV at the S-DALINAC facility [12]. In addition to the previously known dipole states, Pai *et al.* have added 14 new dipole states in their investigation with much improved decay-characteristic values [12]. For some of these states, parity assignments were available from earlier measurements [19–22]. Because of the incomplete parity information, only limited conclusions could be drawn in this recent work [12]. For parity assignments of all the observed dipole states reported in Ref. [12] for ^{52}Cr, we used linearly polarized photon beams at energies of 5.21, 5.56, 6.40, 6.50, 7.00, 7.08, 7.19, 7.40, 7.51, 7.74, 7.89, 8.02, 8.11, 8.20, 8.75, 8.95, 9.15, 9.25, 9.36, and 9.45 MeV and a natural Cr target. Identification of the dipole states was done using the previous unpolarized (γ,γ') measurements [12]. Surprisingly, in our present work, we have not observed the dipole states at $E_x = 5213.7$ and 5526.0 keV that were seen in the previous work. The intensity reported by Pai *et al.* for γ-ray transitions from these states is about half of that found for the transition at $E_\gamma = 5098.6$ keV [12]. We have observed the 5098.6-keV γ-ray transition with good statistics, and based on intensity arguments we should have seen the γ-ray transitions of energies 5213.4 and 5525.7 keV in our spectra. Based on our nonobservation, we argue that these transitions are either inelastic or due to contaminants in the target.

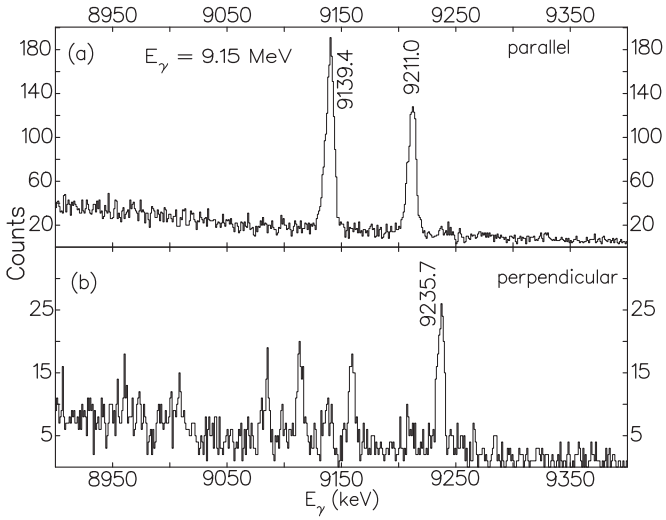

FIG. 2. Same as Fig. 1, at $E_\gamma = 9.15$ MeV.

Figures 1 and 2 show parts of the photon-scattering spectra of the detectors parallel to the polarization plane of the HIγS photon beam and perpendicular to it at incident photon energies of 7.89 and 9.15 MeV, respectively. From these figures it is clear that the transitions at energies of 7864.5, 9139.4, and 9211.0 keV are of an $M1$ nature, whereas the transitions at energie of 7731.3, 7896.8, and 9235.7 keV are of an $E1$ character.

Figure 3 depicts the measured values of the azimuthal intensity asymmetries for ground-state transitions in the energy range of our experiment. The mean values of the azimuthal intensity asymmetry for $J^\pi = 1^+$ and $J^\pi = 1^-$ states are 0.75(7) and $-0.85(9)$, respectively. As shown in Fig. 3, the data are separated depending on their multipolarities ($M1$ or $E1$). The deviation of the azimuthal asymmetry values from the theoretical values of ± 1 is mainly due to the finite geometry of the detector-target arrangement.

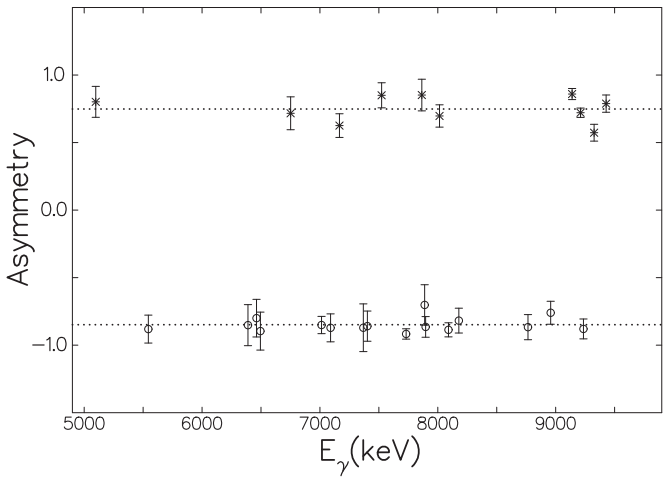

FIG. 3. Experimental azimuthal asymmetry values for $E1$ (open circles) and $M1$ (asterisks) transitions in ^{52}Cr. Average values for $E1$ and $M1$ transitions are drawn as dotted horizontal lines.

TABLE I. Measured asymmetries ϵ and parity quantum number assignments for $J = 1$ states in ^{52}Cr. The asymmetries are not corrected for the finite size of the detectors or attenuation effects. Measured values of $B(M1)\uparrow$ and $B(E1)\uparrow$ are taken from Ref. [12].

E_x (keV)	E_γ (keV)	J^π	ϵ	$B(M1)\uparrow$ (μ_N^2)	$B(E1)\uparrow$ ($10^{-3}\ e^2$ fm^2)
5098.6	5098.4	1^+	0.80(11)	0.089(21)	
5544.7	5544.4	1^-	−0.88(10)		1.88(12)
6389.9	6389.5	1^-	−0.85(29)		0.762(77)
6462.4	6462.0	1^-	−0.80(18)		0.784(78)
6495.5	6495.1	1^-	−0.90(14)		1.367(96)
6752.0	6751.5	1^+	0.72(12)	0.075(9)	
7014.1	7013.6	1^-	−0.85(06)		1.74(25)
7090.8	7090.3	1^-	−0.87(10)		0.496(88)
7166.2	7165.7	1^+	0.63(09)	0.038(8)	
7368.8	7368.2	1^-	−0.87(26)		1.64(13)
7403.2	7402.6	1^-	−0.86(11)		0.76(11)
7524.1	7523.5	1^+	0.85(09)	0.243(18)	
7731.9	7731.3	1^-	−0.92(04)		5.96(40)
7865.1	7864.5	1^+	0.85(12)	0.232(15)	
7889.0	7888.4	1^-	−0.70(21)		2.80(26)
7897.4	7896.8	1^-	−0.86(08)		19.7(10)
8015.3	8014.6	1^+	0.70(08)	0.131(30)	
8091.3	8090.6	1^-	−0.89(05)		3.97(24)
8179.2	8178.5	1^-	−0.82(09)		4.72(98)
8765.9	8765.1	1^-	−0.87(09)		1.88(17)
8958.4	8957.6	1^-	−0.76(09)		0.93(15)
9140.3	9139.4	1^+	0.86(04)	0.898(53)	
9211.9	9211.0	1^+	0.72(03)	0.700(47)	
9236.6	9235.7	1^-	−0.88(07)		1.83(20)
9327.0	9326.1	1^+	0.57(06)	0.238(26)	
9429.0	9428.1	1^+	0.79(06)	0.295(35)	

From the present measurement using polarized photon beams, of the 26 observed dipole excitations in the range of $E_x = 5.1$–9.5 MeV, 16 states were found to be 1^- and 10 states were assigned as 1^+. The measured azimuthal asymmetries ϵ and parity quantum numbers are listed in Table I. The experimental strength distribution values are taken from an earlier work [12].

A. $E1$-strength distribution for ^{52}Cr

The electric dipole excitation-strength distribution of the 16 $J^\pi = 1^-$ states observed in the present work is shown in Fig. 4. The corresponding summed $E1$ strength at $E_x = 5.1$–9.5 MeV in ^{52}Cr is $\sum B(E1)\uparrow = 51.2(16) \times 10^{-3}\ e^2$ fm^2. The lowest-lying candidate for a $J^\pi = 1^-$ level in ^{52}Cr is observed at 5544.7 keV. This level has been investigated as a potential candidate for quadrupole-octupole two-phonon character [22]. The major part of the observed $\sum B(E1)\uparrow$ in ^{52}Cr is distributed at ∼8-MeV excitation energy, with the strongest $E1$ transition at $E_x = 7897.4$ keV. The $B(E1)\uparrow$ value for this transition is $19.7(10) \times 10^{-3}\ e^2$ fm^2, which exhausts almost 40% of the total $B(E1)$ strength and 0.3% of the Thomas-Reiche-Kuhn (TRK) sum rule as reported in Ref. [12].

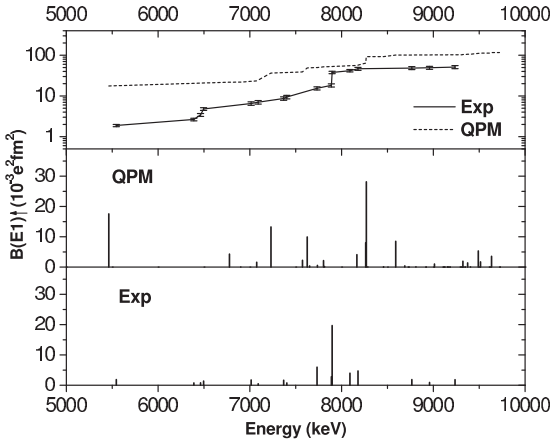

FIG. 4. The distribution of observed $B(E1)\uparrow$ [12] strength for resonantly excited states in ^{52}Cr between 5.1 and 9.5 MeV is compared with values obtained from QPM calculations. A comparison of the measured and calculated QPM cumulative $E1$ strengths is shown in the upper panel. Individual contributions and uncertainties are listed in Table I.

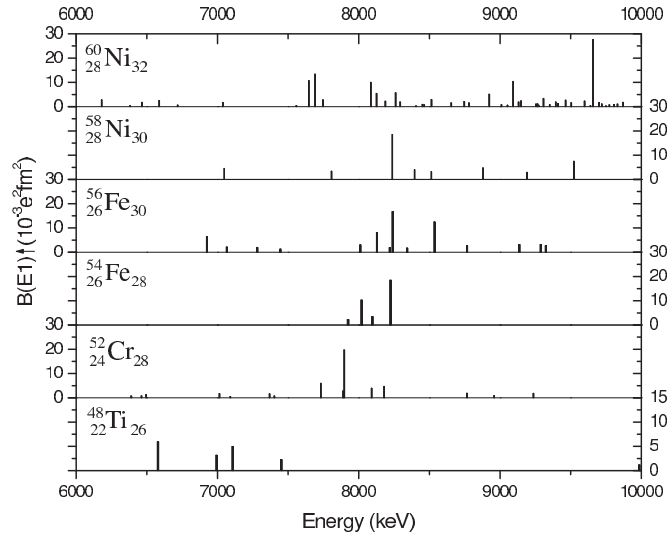

FIG. 5. Distribution of observed $E1$ excitation strength in several fp-shell nuclei. Note the range of the y axis for ^{48}Ti.

Pai *et al.* have suggested ≈0.15% of the TRK sum rule by considering the states at $E_x = 7368.8, 7731.9, 7889.0, 8015.3, 8091.3$, and 8179.2 keV to be $J^\pi = 1^-$ states [12]. In our present measurement using polarized photon beams, we have found that the multipolarity of the level at $E_x = 8015.3$ keV is $J^\pi = 1^+$ instead of $J^\pi = 1^-$, as assumed by Pai *et al.* [12].

Similar strong $E1$ transitions have been seen in the nearby nuclei with $N \approx Z \approx 28$. In $^{58}_{28}$Ni$_{30}$, the strongest $E1$ transition, at $E_x = 8237.3$ keV, corresponds to $B(E1)\uparrow = 18.51(28) \times 10^{-3}\ e^2\,\mathrm{fm}^2$, which is almost one-third of the total identified $E1$ strength [24]. When we move to the $Z = 26$ isotone (i.e., $^{56}_{26}$Fe$_{30}$), the strongest $E1$ transition by far turned out to be at the excitation energy of $E_x = 8239.6$ keV [23], very close to that of ^{58}Ni. The $B(E1)\uparrow$ value corresponding to this transition is $16.69(41) \times 10^{-3}\ e^2\,\mathrm{fm}^2$. As shown in Fig. 5, the strongest transition in ^{56}Fe is accompanied by two smaller fragments at 8127.7 and 8536.3 keV, respectively. These three transitions alone correspond to one-half the total $E1$ strength. The systematics of the distribution of the $B(E1)$ in several fp-shell nuclei is shown in Fig. 5, which is very similar to Fig. 10 in Ref. [24], but with the updated data available for ^{60}Ni [25], ^{56}Fe [23], and ^{52}Cr (present work). In this comparison, we clearly see the similar pattern of strong $E1$ transitions in ^{54}Fe and ^{52}Cr. As pointed out by Bauwens *et al.* [24], this systematics seems to be broken for ^{60}Ni and ^{48}Ti, nuclei farther away from closed shells.

B. $M1$-strength distribution for ^{52}Cr

In the present measurement $M1$ excitations are observed at excitation energies between 5.1 and 9.5 MeV, with a strong concentration of $M1$ strength around 9.2 MeV, as shown in Fig. 6.

A weak and broad concentration of $M1$ strength is found at energies of ∼7.5 MeV. Below 6.75 MeV, there is only one $J^\pi = 1^+$ state, at the excitation energy of ∼5.1 MeV. The total $B(M1)\uparrow$ value in the energy range of our experimental work ($E_x = 5.1$ to 9.5 MeV) is $2.94(9)\mu_N^2$. Magnetic dipole excitations in ^{52}Cr and other $N = 28$ isotones were investigated by Sober *et al.* [19]. According to their work the $M1$ strength distribution in ^{52}Cr is highly fragmented in the energy range of $E_x = 7$–12 MeV, with three distinct energy regimes. Using electron scattering, Sober *et al.* have observed many $J^\pi = 1^+$ states in ^{52}Cr with different levels of confidence for the multipolarity assignments [19]. We have not observed any $J^\pi = 1^+$ states in the 8.1- to 9.0-MeV region, where Sober *et al.* reported many $J^\pi = 1^+$ states, some of them with *unique* multipole assignments [19]. Based on the confidence level of multipolarity assignment for the $M1$

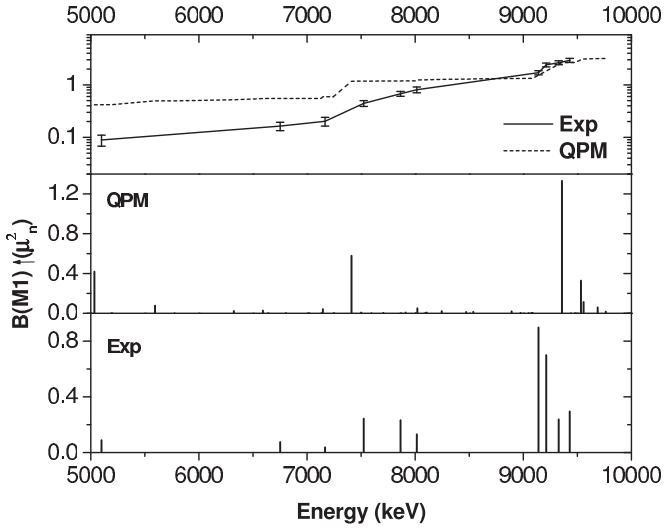

FIG. 6. Distribution of observed $B(M1)\uparrow$ [12] strength in ^{52}Cr in the energy range between 5.1 and 9.5 MeV is compared with the values obtained from QPM calculations. A comparison of the measured and calculated QPM cumulative $M1$ strength is shown in the upper panel. Individual contributions and uncertainties are given in Table I.

transitions and detection limitation, Sober *et al.* recommended a total $M1$ strength value of $8.1(8)\mu_N^2$ in the excitation region of 7–12 MeV. This value is highly suppressed with respect to their shell-model calculations [19]. The total measured $M1$ strength $\sum B(M1)\uparrow$ value decreases to $5.64(22)\mu_N^2$ if only the $M1$ states with *unique* multipolarity assignments are considered. If we consider the $J^\pi = 1^+$ states observed in the present work, the total $M1$ strength is $3.21(13)\mu_N^2$, which is very close to the value reported by Pai *et al.* [12]. In 1998, von Neumann-Cosel *et al.* [9] performed shell-model calculations for the $M1$ strength distribution in ^{52}Cr, as well as in other $N = 28$ isotones, namely, ^{48}Ca, ^{50}Ti, and ^{54}Fe. The total $B(M1)$ strength in ^{52}Cr, using the bare g factor, is $15.60\mu_N^2$. The ratio of the measured to the calculated $B(M1)$ strength, commonly termed the quenching factor, was found to be 0.75 [9] for the $N = 28$ isotones. In ^{48}Ca ($N = 28$, $Z = 20$) the $M1$ strength is essentially concentrated in a single transition at $E_x = 10.23$ MeV, with $\sum B(M1)\uparrow = 4.0(3)\mu_N^2$. If we look at the other $N = 28$ isotones, the strongest $M1$ transitions occur at $E_x = 8.56$, 9.14, and 10.53 MeV in ^{50}Ti, ^{52}Cr, and ^{54}Fe, respectively. The excitation energy of the strongest $M1$ transition in these nuclei moves to higher energies as Z increases from 22 to 26, i.e., more protons are available in the fp shell. In 2006 Li *et al.* provided the first evidence for a spin-flip $M1$ resonance in ^{40}Ar using polarized beams of an energy between 7.7 and 11.0 MeV produced at the HIγS facility [26]. The $M1$ state was found at $E_x = 9.757$ MeV, and the corresponding $B(M1)$ strength value is $0.148(59)\mu_N^2$.

In fp-shell nuclei near $N = Z$, the structure of $M1$ resonances is expected to be dominated by $1p1h$ spin-flip excitations, such as $1f_{7/2} \rightarrow 1f_{5/2}$, for both protons and neutrons. On the upper side of the fp-shell nuclei with $A \sim 60$, the $M1$ strength distribution is somewhat scattered, as expected for semimagic nuclei [23–25]. The distribution of $M1$-excitation strengths for $^{56}_{26}$Fe$_{30}$, $^{58}_{28}$Ni$_{30}$, and $^{60}_{28}$Ni$_{32}$ ($N \approx Z \approx 28$) is shown in Fig. 9 of Ref. [25]. The two accumulations of $J^\pi = 1^+$ states in these nuclei at energies of around 8- and 9-MeV excitation correspond to isoscalar and isovector spin-flip $M1$ resonances [1,25].

IV. THEORETICAL APPROACH AND ANALYSIS OF THE $E1$ AND $M1$ EXPERIMENTAL DATA FOR ^{52}Cr

To interpret the experimentally observed electric and magnetic dipole strength distributions of ^{52}Cr, a detailed treatment of the multiquasiparticle and multiphonon structure of the low-energy 1^+ and 1^- excited states is required. To investigate the spectral fragmentation pattern of the $M1$ and $E1$ strength functions below and around the neutron-emission threshold ($S_n = 12.034$ MeV), calculations in the framework of the nuclear EDF theory for the description of the nuclear ground state [27] and an extended version of the QPM [13,14,28] have been performed. Consistent with previous investigations of $E1$, $E2$, and $M1$ strength functions in various nuclei [3,6,14,29–32], the present QPM calculations are performed with single-particle energies obtained in a self-consistent manner from our EDF approach linked to fully self-consistent Hartree-Fock-Bogoliubov (HFB) calculations [13,14,27]. The excited states are calculated with a residual interaction represented in separable form. The strength parameters are fixed empirically for $E1$ calculations [28,33]. In the case of $M1$ they were obtained from QRPA calculations performed within the density matrix expansion discussed in Ref. [27]. As a further advantage over other QRPA models, the QPM approach incorporates a multiphonon model space built of natural and unnatural parity states. Here, the model basis is constructed of one-, two-, and three-phonon (microscopically described) configurations with J^π ranging from $1^\pm$ to $6^\pm$ and excitation energies E_x up to 9.8 MeV, in agreement with the range of the experimental data. In this sense our QPM calculations are considerably more elaborate than those reported by Pai *et al.* in Ref. [12]. More details on the comparison are given in Ref. [34].

Systematic QRPA and QPM calculations of the electric dipole response in different isotopic and isotonic chains of nuclei [13,14,29,30,32] indicate enhanced $E1$ strength in the energy range below the neutron threshold with respect to the shape of a Lorentz-like strength function used to analyze the GDR [32,35]. A common observation is that the total $E1$ QRPA strength associated with the PDR increases with an increase in the isospin asymmetry of the nucleus defined by the N/Z ratio. In this connection, a correlation between the total PDR strength obtained in QRPA calculations and the neutron skin thickness [13,14,29,30], which in neutron-rich nuclei is defined by the difference between neutron and proton root-mean-square radii, $\delta r = \sqrt{\langle r^2\rangle_n} - \sqrt{\langle r^2 >_p\rangle}$, is found [13,14,29,30]. Similar results are also obtained from various experiments [2].

From our EDF mean-field calculations we derive that the ^{52}Cr nucleus exhibits a neutron skin with a thickness of $\delta r = 0.056$ fm. As a result, the first QRPA 1^-_1 state, with excitation energy $E_x = 8.366$ MeV, and the second QRPA 1^- state, with excitation energy $E_x = 9.473$ MeV, are almost-pure neutron two-quasiparticle states, where the major contribution is due to transitions from weakly bound orbitals: $1d_{3/2} \rightarrow 2p_{3/2}$, $2s_{1/2} \rightarrow 2p_{3/2}$, and $1f_{7/2} \rightarrow 1g_{9/2}$. Taking into account these considerations, the energy range below ~9.5 MeV could be associated with a genuine PDR mode. Theoretically, this can be seen also from the evolution of the proton and neutron transition densities, which show a behavior typical for PDR nuclei [14,32]. The total PDR strength obtained from the QRPA calculations in ^{52}Cr is $\Sigma_{0\,\mathrm{MeV}}^{9.5\,\mathrm{MeV}} B(E1; \mathrm{g.s.} \rightarrow 1^-_{\mathrm{PDR}})_{\mathrm{QRPA}}\uparrow = 13 \times 10^{-3}\ e^2\,\mathrm{fm}^2$, which exhausts about 0.1% of the TRK sum rule.

As the excitation energy is increased, the isovector contribution to the dipole strength increases, and the structure of the state vectors shows an increase in the out-of-phase neutron-to-proton contribution and related energy-weighted sum rules, which is generally associated with the GDR [14,32]. The corresponding strength function begins to follow closely its Lorentzian fall-off, often assumed for the GDR in data analyses [35].

Theoretically, it is clear that the QRPA is unable to account for higher multiparticle-multihole correlations and interactions resulting from core polarization effects [36]. The latter could induce dynamical effects related to redistribution

of strength and strongly affect the gross and fine structure of dipole strength functions. By comparing the QRPA with the multiphonon QPM calculations, it is seen that the pure two-quasiparticle QRPA strengths in the PDR region are strongly fragmented over many 1^- excited states, once the coupling to multiphonon configurations takes place. The lowest-lying 1^- state, which is without a QRPA counterpart, is predominantly given by a two-phonon quadrupole-octupole excitation [37] of the $[2^+_1 \otimes 3^-_1]$ configuration, which accounts for ≈75% of the QPM wave function. These results are obtained when the QPM multiphonon basis is truncated at 9 MeV. In this case the calculated value for the energy of the 1^-_1 state is $E_{\rm QPM} = 5.61$ MeV, and the reduced transition probability is $B(E1; \text{g.s.} \rightarrow 1^-_1)_{\rm QPM} \uparrow = 6.66 \times 10^{-3}\ e^2\,\text{fm}^2$. In comparison, the experimental values are $E_{\rm exp} = 5.545$ MeV and $B(E1; \text{g.s.} \rightarrow 1^-_1)_{\rm exp} \uparrow = 1.88(12) \times 10^{-3}\ e^2\,\text{fm}^2$. The collectivity of the 1^-_1 state strongly depends on the model configuration space used in the calculations. The increase in the energy range of the two- and three-phonon configurations up to 9.8 MeV leads to a more collective 1^-_1 state with a lower excitation energy, $E_{\rm QPM} = 5.463$ MeV and $B(E1; \text{g.s.} \rightarrow 1^-_1)_{\rm QPM} \uparrow = 17.56 \times 10^{-3}\ e^2\,\text{fm}^2$. The strongest QPM $1^-_{\rm max}$ state in the energy range below 9.8 MeV is located at $E_{\rm QPM} = 8.270$ MeV and the corresponding transition probability is $B(E1; \text{g.s.} \rightarrow 1^-_{\rm max})_{\rm QPM} \uparrow = 28.14 \times 10^{-3}\ e^2\,\text{fm}^2$. The theoretical results compare well with the experimental findings, which give for this state $E_{\rm exp} = 7.897$ MeV and $B(E1; \text{g.s.} \rightarrow 1^-_{\rm max})_{\rm QPM} \uparrow = 19.7(10) \times 10^{-3}\ e^2\,\text{fm}^2$, and also with the QPM calculations of Pai *et al.* [12]. The QPM calculations indicate that the $1^-_{\rm max}$ state contains contributions from the low-energy tail of the GDR, which is the reason for the strong $B(E1)$ transition rate.

Furthermore, the 1^- states associated with the PDR mode in ^{52}Cr are widely distributed in the energy range $E_x \approx 6.6$–11.6 MeV. The structure of these states incorporates decay fragments of the 1^-_1 and 1^-_2 QRPA states, related to the PDR mode, but it also contains contributions of multiphonon components and core polarization effects from GDR. As a result, the three-phonon QPM calculations give a much more low-energy $B(E1)$ strength than obtained for the QRPA pure PDR strength. The experimental data also show a sequence of states in the theoretical predicted PDR energy range, but they are more fragmented.

For the whole measured energy range, $E_x = 5.1$–9.5 MeV, the QPM calculations predict a summed $B(E1)$ strength of $\sum B(E1)_{\rm QPM} \uparrow = 111 \times 10^{-3}\ e^2\,\text{fm}^2$. In comparison, the experiment finds $\sum B(E1)_{\rm exp} \uparrow = 51.2(16) \times 10^{-3}\ e^2\,\text{fm}^2$, a factor of ∼2 less strength.

The comparison between the measurements and the QPM calculations of the cumulative $B(E1)$ strength and the spectral distribution in ^{52}Cr is presented in the upper panel in Fig. 4. In general, the shape of the QPM cumulative $B(E1)$ strength as well as the 1^- level distribution is found to be in very good agreement with the experimental data. The observed difference between the measured and the calculated total $B(E1)$ values could be related to the experimental sensitivity limits and branchings to excited states, which are unaccounted for by the existing dipole data on ^{52}Cr. In this connection, the experimental value for the total $B(E1)$ strength represents a lower limit only. More details on this issue are discussed in [3,34] and [38]. For example, cascade simulations for the ^{90}Zr nucleus described in Ref. [6] give a 76(10)% mean branching ratio for ground-state transitions of 1^+ levels for excitation energies below 10 MeV, resulting in an increase in the measured total $B(M1)$ strength of about 25%.

In Ref. [6], the quenching phenomenon of the nuclear spin-flip magnetic response of ^{90}Zr was investigated. Theoretically, the description of the fine structure of the $M1$ strength requires the analysis of the complete spectrum of 1^+ excited states by accounting for core polarization effects. The latter contributions were successfully described by the three-phonon QPM [3,6]. In contrast to many other approaches in which the genuine many-body effects originating from core polarization are left unaccounted for, in our approach the deviation of static and transition magnetic moments from the accepted values could be attributed mainly to mesonic and subnucleonic contributions to the transition operators [39,40]. These effects, coming from hard processes, are connected with energy and momentum scales much different from the nuclear low-energy region. Schematically, they are taken into account by a renormalization of the spin-g factor whose "quenched" value should be related to the lower limit of the quenching, indicating the amount of strength located outside the model space and, also, accounting for the contributions from the hard scale of mesonic and subnucleonic degrees of freedom. Hence, following previous QPM calculations [33], the $M1$ transitions are calculated with a quenched effective spin-magnetic factor $g^s_{\rm eff} = 0.8 g^s_{\rm bare}$, where $g^s_{\rm bare}$ denotes the bare spin-magnetic moment. This value agrees very well with shell-model calculations and the experimental data for $N = 28$ nuclei from Refs. [9] and [41], where $g^s_{\rm eff} = 0.75 g^s_{\rm bare}$ is obtained. In particular, from a comparison to Gammow-Teller strengths in various fp-shell $N = 28$ nuclei extracted from charge-exchange reactions, Monte Carlo shell-model studies [42] support our value of $g^s_{\rm eff} = 0.8 g^s_{\rm bare}$, however, with uncertainties of about 20%. In contrast, in the QPM calculations of Pai *et al.* [12] the smaller value of $g^s_{\rm eff} = 0.6 g^s_{\rm bare}$ was used in order to reproduce the experimental $M1$ data in ^{52}Cr, which were theoretically overestimated otherwise.

A reliable description of the fragmentation pattern of the magnetic dipole ($M1$) response function is important for understanding the spin dynamics of the nucleus. The analysis of the QRPA $M1$ strength of 1^+ excitations with energies up to $E_x = 20$ MeV indicates that this part of the spectrum is mostly due to single p-h excited states of the spin-flip type related to the excitation of neutron and proton $1f_{7/2} \rightarrow 1f_{5/2}$ two-quasiparticle components, respectively. The latter dominate the structure of the first two lowest-lying QRPA 1^+ excited states, the 1^+_1 state at $E_x = 8.92$ MeV and the 1^+_2 state at $E_x = 10.53$ MeV, which share more than 95% of the total $B(M1) \uparrow = 10.3 \mu^2_N$ up to $E_x = 20$ MeV. In the excitation energy range between 10 and 20 MeV we find also contributions of $1d_{5/2} \rightarrow 1d_{3/2}$, $2p_{3/2} \rightarrow 2p_{1/2}$, $1d_{3/2} \rightarrow 2d_{5/2}$, $1p_{1/2} \rightarrow 2p_{3/2}$, and $1p_{3/2} \rightarrow 2p_{1/2}$ transitions. For comparison, the shell-model calculations in Refs. [9] and [41] include the valance fp shells only.

Including only the orbital term of the nuclear magnetic moment in the QPRA calculations, we obtain the pure orbital QPRA $M1$ strength. It is found to be very small, approximately 3.3% of the total QPRA $B(M1)$ transition probability, which includes both spin-flip and orbital contributions up to $E_x = 20$ MeV. In general, the interference between spin-flip and orbital $M1$ strengths leads to the suppression of the total $M1$ response, as also reported in [6].

Detailed studies of the $M1$ fragmentation pattern based on three-phonon QPM calculations show that the coupling of natural-parity phonons to multiphonon 1^+ states induces additional orbital contributions to the $M1$ transitions. Consequently, the observed $M1$ strength at excitation energies between 5 and 10 MeV contains an orbital part of about 11%, which is less than that found for the case of ^{90}Zr [6]. The excited 1^+ states at about $E_x = 5$ MeV contain mainly orbital contributions. For higher-lying 1^+ states the spin-flip part of the wave function is dominant.

In general, the multiphonon QPM calculations indicate that the $M1$ strength distribution below $E_x = 10$ MeV could be related to fragmentation of the 1^+_1 and 1^+_2 QRPA states. Thus, in this energy region about 90% of the fragmented first QRPA 1^+_1 and only about 5% of the fragmented second QRPA 1^+_2 state are located. The latter makes a significant contribution to the $M1$ spin-flip strength at energies above 10 MeV, the energy range which includes the neutron-separation energy as well. Experimentally, it is a formidable task to distinguish these 1^+ states in the vicinity of the neutron threshold from background components and the GDR. However, we can explore this region theoretically in the QPM. The model predicts strongly fragmented $M1$ strength, related mainly to the decay of the 1^+_2(QRPA) state over a considerable number of 1^+ states with relatively low transition probabilities and a total $\Sigma_{10\,\mathrm{MeV}}^{12.5\,\mathrm{MeV}} B(M1)\uparrow$ of $\approx 6\mu_N^2$. This is a considerable amount of $M1$ strength, which deserves further experimental attention.

The total QPM $M1$ strength summed over 1^+ states from $E_x = 5$ MeV to $E_x = 9.5$ MeV can be compared directly with the present data. The results are presented in Fig. 6. The theoretical findings give $\Sigma_{5\,\mathrm{MeV}}^{9.5\,\mathrm{MeV}} B(M1)_{\mathrm{QPM}}\uparrow = 3.1\mu_N^2$, which is in good agreement with the experimental value of $\Sigma_{9.5\,\mathrm{MeV}}^{5.1\,\mathrm{MeV}} B(M1)_{\mathrm{exp}}\uparrow = 2.94(9)\mu_N^2$. However, one should take into account that this experimental value for the $B(M1)$ strength does not include the contributions of branchings to excited states, which might increase the measured total $M1$ strength.

V. CONCLUSIONS

^{52}Cr(γ,γ') photon scattering experiments have been performed using the nearly monoenergetic, 100% linearly polarized photon beams produced at the HIγS facility of TUNL. Twenty beam energies have been used to cover the energy range from 5.0 to 9.5 MeV and to uniquely identify and measure the dipole excitations in ^{52}Cr. Twenty-six dipole excitations were identified and their parity quantum values were unambiguously determined from the measured azimuthal intensity asymmetry of nuclear resonance fluorescence transitions. The distributions of magnetic and electric excitations have been discussed in detail with experimentally measured (from Ref. [12]) values of $\sum B(E1)\uparrow = 51.2(16)\times 10^{-3}\ e^2\,\mathrm{fm}^2$ and $\sum B(M1)\uparrow = 2.94(9)\mu_N^2$.

From three-phonon QPM calculations of the electric dipole response in ^{52}Cr, specific signals of a new mode of excitation related to PDR are observed. As a common feature in neutron-rich nuclei, the structure of the PDR excited states in ^{52}Cr is dominated by neutron components directly connected to the presence of a neutron skin. The generic character of the PDR is further confirmed by the investigation of related transition densities. The PDR energy location and its total $B(E1)$ strength are predicted.

The observation of the spin-flip $M1$ resonance structure around 9.1 MeV in ^{52}Cr has been discussed along with the systematics of the distribution of dipole excitation in fp-shell nuclei. Such a concentration of $M1$ strength around 9.2 MeV is further confirmed in three-phonon QPM calculations and explained as fragmented spin-flip 1^+ excitations.

In these studies a common observation is that the QRPA is unable to describe the low-energy nuclear dipole response in detail. This can be achieved only if one takes into account the contribution of multiphonon coupling, which explains the observed fragmentation pattern of the $E1$ and $M1$ strengths and their absolute value. In addition, the theoretical investigations of the fragmentation pattern of the $M1$ strength indicate that the contribution of the orbital part of the magnetic moment is mainly due to coupling of multiphonon states. The effect is estimated to account for about 11% of the total $M1$ strength below the neutron-emission threshold. The good agreement of the calculated and measured total $M1$ strength is a signature that the quenching is handled reliably in the chosen approximation. A better understanding could be achieved with more comprehensive knowledge of the nature of the intrinsic nuclear moments, meson-exchange currents, and branching ratios from excited states, which might be of importance for further improvements.

ACKNOWLEDGMENTS

We are grateful to the HIγS staff for providing excellent photon beams during our experiments. This work was supported by U.S. Department of Energy Grant No. DE-FG02-97ER41033 and BMBF Grant No. 05P12RGFTE.

[1] K. Heyde, P. von Neumann Cosel, and A. Richter, Rev. Mod. Phys. **82**, 2365 (2010).
[2] D. Savran, T. Aumann, and A. Zilges, Prog. Part. Nucl. Phys. **70**, 210 (2013).
[3] A. Tonchev *et al.*, Phys. Rev. Lett. **104**, 072501 (2010).
[4] N. Pietralla, Z. Berant, V. N. Litvinenko, S. Hartman, F. F. Mikhailov, I. V. Pinayev, G. Swift, M. W. Ahmed, J. H. Kelley, S. O. Nelson, R. Prior, K. Sabourov, A. P. Tonchev, and H. R. Weller, Phys. Rev. Lett. **88**, 012502 (2001).
[5] M. Arnould and S. Goriely, Phys. Rep. **384**, 1 (2003).

[6] G. Rusev *et al.*, Phys. Rev. Lett. **110**, 022503 (2013).
[7] W. Steffen *et al.*, Phys. Lett. B **95**, 23 (1980).
[8] V. Derya *et al.*, Phys. Lett. B **730**, 288 (2014).
[9] P. von Neumann-Cosel, A. Poves, J. Retamosa, and A. Richter, Phys. Lett. B **443**, 1 (1998).
[10] A. Richter, Prog. Nucl. Part. Phys. **13**, 1 (1984).
[11] A. Bohr and B. R. Mottelson, *Nuclear Structure* (Benjamin, New York, 1975).
[12] H. Pai *et al.*, Phys. Rev. C **88**, 054316 (2013).
[13] N. Tsoneva, H. Lenske, and Ch. Stoyanov, Phys. Lett. B **586**, 213 (2004).
[14] N. Tsoneva and H. Lenske, Phys. Rev. C **77**, 024321 (2008), and refs. therein.
[15] H. R. Weller, M. W. Ahmed, H. Gao, W. Tornow, Y. K. Wu, M. Gai, and R. Miskimen, Prog. Part. Nucl. Phys. **62**, 257 (2009).
[16] S. L. Hammond, A. S. Adekola, C. T. Angell, H. J. Karwowski, E. Kwan, G. Rusev, A. P. Tonchev, W. Tornow, C. R. Howell, and J. H. Kelley, Phys. Rev. C **85**, 044302 (2012).
[17] P. M. Goddard *et al.*, Phys. Rev. C **88**, 064308 (2013).
[18] C. Romig *et al.*, Phys. Rev. C **88**, 044331 (2013).
[19] D. I. Sober, B. C. Metsch, W. Knüpfer, G. Eulenberg, G. Küchler, A. Richter, E. Spamer, and W. Steffen, Phys. Rev. C **31**, 2054 (1985).
[20] N. Kumagai *et al.*, Nucl. Phys. A **329**, 205 (1979).
[21] U. E. P. Berg *et al.*, Phys. Lett. B **103**, 301 (1981).
[22] J. Enders *et al.*, Nucl. Phys. A **636**, 139 (1998).
[23] T. Shizuma, T. Hayakawa, H. Ohgaki, H. Toyokawa, T. Komatsubara, N. Kikuzawa, T. Inakura, M. Honma, and H. Nakada, Phys. Rev. C **87**, 024301 (2013).
[24] F. Bauwens, J. Bryssinck, D. De Frenne, K. Govaert, L. Govor, M. Hagemann, J. Heyse, E. Jacobs, W. Mondelaers, and V. Yu. Ponomarev, Phys. Rev. C **62**, 024302 (2000).
[25] M. Scheck *et al.*, Phys. Rev. C **88**, 044304 (2013).
[26] T. C. Li *et al.*, Phys. Rev. C **73**, 054306 (2006).
[27] F. Hofmann and H. Lenske, Phys. Rev. C **57**, 2281 (1998).
[28] V. G. Soloviev, *Theory of Complex Nuclei* (Pergamon Press, Oxford, UK, 1976).
[29] S. Volz *et al.*, Nucl. Phys. A **779**, 1 (2006).
[30] R. Schwengner *et al.*, Phys. Rev. C **78**, 064314 (2008).
[31] N. Tsoneva and H. Lenske, Phys. Lett. B **695**, 174 (2011).
[32] R. Schwengner *et al.*, Phys. Rev. C **87**, 024306 (2013).
[33] A. I. Vdovin, V. V. Voronov, V. Yu. Ponomarev, and Ch. Stoyanov, Yad. Fiz. **30**, 923 (1979) [Sov. J. Nucl. Phys. **30**, 479 (1979)].
[34] B. Özel-Tashenov *et al.*, Phys. Rev. C **90**, 024304 (2014).
[35] B. L. Berman, At. Data Nucl. Data Tables **15**, 319 (1975).
[36] N. Tsoneva and H. Lenske, EPJ Web Conf., (2015); www.epj-conferences.org.
[37] V. Yu. Ponomarev, Ch. Stoyanov, N. Tsoneva, and M. Grinberg, Nucl. Phys. A **635**, 470 (1998).
[38] D. Savran *et al.*, Phys. Rev. Lett. **100**, 232501 (2008).
[39] A. Arima and H. Horie, Prog. Theor. Phys. **11**, 509 (1954).
[40] A. Arima, Hyperfine Interact. **78**, 67 (1993).
[41] K. Langanke, G. Martinez-Pinedo, P. von Neumann-Cosel, and A. Richter, Phys. Rev. Lett. **93**, 202501 (2004).
[42] S. E. Koonin, D. J. Dean, and K. Langanke, Annu. Rev. Nucl. Part. Sci. **47**, 463 (1997).